Warm Season Subseasonal Variability and Climate Extremes in the Northern Hemisphere: The Role of Stationary Rossby Waves

Siegfried Schubert, Hailan Wang[1], and Max Suarez

Global Modeling and Assimilation Office
NASA GSFC, Greenbelt, Maryland

20 December 2010

To be submitted to the Journal of Climate
MERRA Special Issue

[1] Also, *Goddard Earth Sciences and Technology Center, University of Maryland at Baltimore County, Baltimore, Maryland*

Abstract

This study examines the nature of boreal summer subseasonal atmospheric variability based on the new NASA Modern-Era Retrospective analysis for Research and Applications (MERRA) for the period 1979-2010. An analysis of the June, July and August subseasonal 250hPa v-wind anomalies shows distinct Rossby wave-like structures that appear to be guided by the mean jets. On monthly subseasonal time scales, the leading waves (the first 10 rotated empirical orthogonal functions or REOFs of the 250hPa v-wind) explain about 50% of the Northern Hemisphere v-wind variability, and account for more than 30% (60%) of the precipitation (surface temperature) variability over a number of regions of the northern middle and high latitudes, including the U.S. northern Great Plains, parts of Canada, Europe, and Russia. The first REOF in particular, consists of a Rossby wave that extends across northern Eurasia where it is a dominant contributor to monthly surface temperature and precipitation variability, and played an important role in the 2003 European and 2010 Russian heat waves. While primarily subseasonal in nature, the Rossby waves can at times have a substantial seasonal mean component. This is exemplified by REOF 4 which played a major role in the development of the most intense anomalies of the U.S. 1988 drought (during June) and the 1993 flooding (during July), though differed in the latter event by also making an important contribution to the seasonal mean anomalies. A stationary wave model (SWM) is used to reproduce some of the basic features of the observed waves and provide insight into the nature of the forcing. In particular, the responses to a set of idealized forcing functions are used to map the optimal forcing patterns of the leading waves. Also, experiments to reproduce the observed waves with the SWM using MERRA-based estimates of the forcing indicate that the wave forcing is dominated by sub-monthly vorticity transients.

1. Introduction

The boreal summer mean extratropical circulation lacks the strong jets and large amplitude stationary waves that typify the boreal winter climate. This, together with the presence of pervasive tropical easterlies that inhibit remote forcing from the tropics, tend to limit the sources of boreal summer middle latitude variability to more local/regional processes, with meso-scale convective weather systems, and land-atmosphere coupling playing important roles (e.g., Parker and Johnson 2000; Koster et al. 2000). Nevertheless, the summer season does exhibit substantial variability on monthly time scales including periods of extreme heat and flooding that appear to, at times, develop as part of continental if not planetary scale circulation changes (e.g., Carril et al. 2007). The nature of such large-scale summer circulation changes, including the mechanisms that act to maintain them on time scales far beyond those of local weather processes, is as yet unclear. One potentially important mechanism is Rossby wave dispersion, in which the jet acts as a waveguide– a process known to be an important source of circumglobal teleconnectivity during the winter (e.g., Hoskins and Ambrizzi, 1993; Branstator 2002).

While summer jets in the upper troposphere are weaker than the typical winter jets, there is now considerable evidence that the meridional gradients and near circumpolar extent of the summer jets can support important guides for Rossby waves. Ambrizzi et al. (1995) summarized the teleconnectivity associated with the boreal summer wave-guides and preferred propagation patterns towards and away from the wave-guides. Newman and Sardeshmukh (1998) examined the seasonality of the Pacific/North American response to remote low-frequency forcing and showed that the changes are tied to the seasonal changes in the shape and location of the Rossby waveguide.

They further showed that the amplitude of the forced response over the United States to forcing over the west Pacific can potentially be larger in June than any other month of the year.

In this study, we take a new look at the large-scale controls of boreal summer (June, July and August or JJA) surface temperature and precipitation variability on subseasonal (30-90 day) time scales using the output from MERRA (Rienecker et al. 2011). The study builds on the results of a number of earlier studies that found that summertime Rossby waves have played an important role in summer climate extremes. For example, Namias (1983; 1991) found that warm season droughts over the US Great Plains (e.g, the 1988 drought) tend to be associated with upper level anti-cyclones linked to standing Rossby wave patterns. Lyon and Dole (1995) showed that both the 1980 and 1988 droughts were associated with anomalous stationary wave patterns, with apparent source regions in the North Pacific. Chen and Newman (1998) suggested that the intense anomalous anticyclones associated with the 1988 drought were linked to propagating Rossby waves originating in the west Pacific. Lau and Weng (2002) and Lau et al. (2004) found that summertime precipitation anomalies over North American and the Asian monsoon regions appear to be linked by wave-train patterns that recur on seasonal to interannual time scales.

Ding and Wang (2004) isolated an interannually varying Northern Hemisphere circumglobal teleconnection (CGT) pattern linked to the Indian monsoon. They found that the CTG has a preferred wave number 5 structure, is primarily confined within the waveguide associated with the NH summer jet stream, and is linked to significant rainfall and surface air temperature anomalies in the continental regions of western Europe, European Russia, India, east Asia, and North America. They suggested that the heat sources associated with the Indian summer

monsoon may be responsible for maintaining the CGT. Wang et al. (2009) found that the abnormally wet conditions in the Central Intermountain West of the United States during June 2009 were associated with a circumglobal teleconnection pattern, which they characterized as a short Rossby wave train along the jet stream waveguide with a wave number 5 structure.

In this study we look more generally at the characteristics of the boreal summer Rossby waves, using MERRA to quantify their structure and their impacts on surface meteorology on subseasonal time scales. A stationary wave model (SWM) is used to characterize the preferred regions of forcing of the leading waves, and provide insights into the nature of the forcing terms. Section 2 describes the data and our diagnostic approach. The results of our diagnostic analysis are presented in Section 3. Section 4 describes the results of the SWM experiments with idealized and MERRA-based estimates of the forcing. The summary and conclusions are given in Section 5.

2. The data and diagnostic approach

The analysis is based on MERRA (Rienecker et al. 2011). MERRA was produced with the Goddard Earth Observing System Data Assimilation System Version 5 (GEOS-5) documented in Rienecker et al. (2008), consisting of the GEOS-5 atmospheric model and the Grid-point Statistical Interpolation (GSI) analysis system, the latter being a system jointly developed by the GMAO and NOAA's National Centers for Environmental Prediction. The GEOS-5 assimilation system includes an incremental analysis update (IAU) procedure (Bloom et al. 1996) that slowly adjusts the model states toward the observed state. This has the benefit of minimizing any unrealistic spin down (or spin-up) of the water cycle. MERRA was run at a resolution of ½°

latitude × 2/3° longitude with 72-levels extending to 0.01hPa. More information about MERRA can be found at: http://gmao.gsfc.nasa.gov/research/merra/. This study uses standard monthly mean (JJA) and hourly output that is provided on 42 pressure levels at a horizontal resolution of 1° latitude × 1.25° longitude for the period 1979-2010.

In addition to MERRA, we make use of other observations consisting of the monthly mean (2.5° latitude by 2.5° longitude) Global Precipitation Climatology Project (GPCP version 2) precipitation data documented in Adler et al. (2003), and the Climate Research Unit (CRU) monthly mean surface air temperature product (Mitchell and Jones 2005). The CRU temperatures (version TS3.0) are on a spatial grid of 0.5° latitude by 0.5° longitude.

The leading patterns of 250mb v-wind subseasonal monthly mean variability are isolated using rotated empirical orthogonal functions (REOFs), where VARIMAX rotation (e.g., Richman 1986) is used to help separate (geographically) the leading wave structures. After some experimentation, we found that rotating the first sixty EOFs produces stable results (rotating more than that has no affect on the leading REOFs). The connections between these patterns of variability and other fields (e.g., precipitation and surface air temperature) are determined using both correlations and linear regression.

The statistical significance of the correlations and regressions is determined using a Monte Carlo approach that mimics the calculations done with the data. For the correlations, we first generate two sets of 96 (3 months times 32 years) independent, identically distributed (iid) normal random variates with zero mean and unit variance. Then, "intraseasonal" anomalies are computed by

removing the average of every set of three iid variates. Next, the correlations between the two sets of anomalies are computed. These steps are repeated 1000 times and the resulting correlations are ordered from smallest to largest. The 25^{th} and 975^{th} values determine the 5% significance levels. For the regressions, the iid variates are scaled to have the same variance as the leading REOFs, and these are then used as the predictors for either precipitation or surface temperature at each gridpoint. This is carried out 1000 times (for every grid point) and the values are sorted from smallest to largest. The 950^{th} (900^{th}) value is the 5% (10%) significance value for each surface temperature (precipitation) regression.

3. Diagnostic Analysis based on MERRA

In this section, we examine the variability of the upper tropospheric circulation on subseasonal time scales for the months of June, July and August (JJA) for the years 1979 -2010. This includes an assessment of the extent to which the circulation changes are linked to surface temperature and precipitation variability. We begin by focusing on the 250hPa meridional wind field – a quantity that provides a clear measure of upper tropospheric wave activity.

Figure 1 shows examples of the spatial structure and time evolution of subseasonal wind variability based on lag-correlations of the 250hPa v-wind with respect to three different base points. The results are based on daily fields that have been band-pass (30-90 day) filtered using a symmetric, 4-pole, low-pass tangent-Butterworth filter (Oppenheim and Schafer 1975). When the base point is located in the central Great Plains, the correlations (at lag zero) show a clear signature of a standing wave that spans much of the western hemisphere and is largely embedded

within the jet stream with a zonal wave number 6 structure. An examination of the time lags reveals that energy is moving through the wave from west to east with a group velocity of 20-25 m/s. Similar results are obtained without filtering (not shown), although the far-field components of the wave are filtered out by the presence of higher frequency waves and the spatial scale is slightly smaller, reflecting the mixing of the results with the shorter spatial scales of the high frequency waves.

The results for a base point over northwestern Russia (middle panels) show a somewhat different behavior, although the wave again has a fixed phase. In this case, the wave energy moves along the North America/Atlantic jet, but then appears to split at the jet exit region, with most of the wave activity moving northeastward out of the jet in a path over northern Eurasia (north of the jet) where it has a zonal wavelength of about 90° longitude. Some of the wave energy moves south and east (initially south over northern Africa), remaining effectively embedded in the Asian jet. The behavior is again similar in the unfiltered data (not shown). The right panels show the structure obtained if the base point is moved south over the Caspian Sea. In that case the wave energy is almost entirely confined to the jet, with the wave extending from Europe across southern Eurasia into the Pacific.

The above results are representative of the structures and evolution obtained using different base points throughout the hemisphere in or near the jets, with most base points showing the wave activity confined to the jet (e.g., left panels of Fig. 1). The main exceptions are the base points near the jet exit region over the North Atlantic where some if not most of the energy appears to propagate out of and to the north of the jets (e.g., middle panels of Fig. 1). We note that results

based on a filter that retains 10-30 days (not shown) also show clear evidence of Rossby waves, although at these time scales the spatial scales are somewhat smaller and there is clear evidence of eastward phase propagation. We will discuss further the characteristics of the stationary Rossby waves in the next section in the context of a stationary wave model.

In the following, we focus the analysis on monthly mean quantities. Our estimate of subseasonal (30-90 day) variability in that case involves the monthly mean deviations from both the long-term mean for each month, and the seasonal (JJA) mean for any particular year. In particular, the total monthly mean variance in V averaged over the summer (JJA) season can be decomposed as follows:

$$\left\langle \overline{\left(V-\overline{V}\right)^2} \right\rangle = \overline{\left\langle V' \right\rangle^2} + \overline{\left\langle V'^{*2} \right\rangle}, \qquad (1)$$

where the overbar denotes the long term mean (1979-2010) for a particular month, and the prime is the deviation from the long term mean. Also, the angle brackets denote a seasonal mean (JJA), and the star is the deviation from the seasonal mean. The first term on the right hand side (RHS) is the variance of the seasonal mean anomalies, while the second term on the RHS is the subseasonal variance – our main focus.

Fig. 2 shows the unbiased estimates[2] of both terms on the RHS of (1). The results show the dominance of the subseasonal variance (top panel of Fig. 2) with relatively high variance extending in bands around the globe in both hemispheres. While the focus here is on the boreal summer, we note that the Southern Hemisphere also shows extensive regions of high subseasonal variability spanning the global at both 30°S and 60°S especially over the Pacific Ocean, consistent with an important role for Rossby waves (e.g. Ambrizzi et al. 1995). In the Northern Hemisphere, local maxima occur over the eastern North Atlantic, Northern Europe, the Ural Mountains, northeastern Russia (just west of the Verhoyansk Mountains), a region just south of the Aleutian Islands, and on both the west and east coasts of North America. There is some evidence of a secondary track of relatively high variance over southern Eurasia with local maxima just west of the Caspian Sea, and again just west of the Tian Shan mountains near 70°E and 40°N. The latter was identified by Ding and Wang (2004) as a potentially important region of interannual variability associated with the circumglobal teleconnection pattern mentioned in the Introduction. Consistent with their results, we also find that region to have substantial interannual variability (bottom panel of Fig 2). In general, the interannual variance of the seasonal mean anomalies is a weaker version of the subseasonal variance, with a geographical distribution that tends to be in quadrature with that of the subseasonal variance (maxima tend to fall to the east of the corresponding subseasonal maxima). The geographical distribution of the variance discussed above, suggests that regions of high topography and possibly land-sea contrasts, may play some role in anchoring the variance.

We next summarize the subseasonal 250mb v-wind variability using rotated empirical

[2] For the sub-seasonal variance it is especially important to use an unbiased estimator since for each year there are only N =3 terms in the sum of squares. The unbiased variance estimate for each year is obtained by dividing the sum of squares by N-1 =2. These are then averaged over 32 years.

orthogonal functions (REOFs, Richmond 1986). Our focus is on the mature stationary Rossby waves, so REOFs should provide a reasonable set of basis functions for isolating any preferred regional development of these waves. Figure 3 shows the five leading REOFs. The first REOF bears a striking resemblance to the lag –zero one-point correlation map shown in the middle panels of Figure 1. The second REOF is centered on the North Pacific region linking Asia with North America, while the third is centered over the North Atlantic, linking North America and Europe. The fourth REOF is centered over North America and is approximately in quadrature with the third, while the fifth REOF spans the Asian continent where it is for the most part embedded in the Asian jet extending from Europe to the North American continent. This REOF bears some resemblance to the interannual CGT found by Ding and Wang (2004) and, as we shall see in Fig. 7, also appears to have an interannual component. Together, the first 5 (10) REOFs explain 1/3 (1/2) of the monthly mean subseasonal variance.

It is not clear to what extent the REOFs can be interpreted as distinct physical modes of variability – something that is difficult to determine by purely statistical measures especially for rotated EOFs (the percent variance explained indicates little separation in variance, ranging from 8.2% for the first to 4.1% for the fifth REOF). Some indication that these patterns represent physical modes of variability is given by the fact that they have counterparts in lag correlation patterns such as those shown in Fig. 1. Also, we will show in the next section that very similar wave structures can be produced, by forcing a stationary wave model with localized vorticity or heat sources.

While the leading REOFs are important contributors to the upper tropospheric variability, it is not clear that they contribute in a significant way to subseasonal variability in surface meteorology. To examine this, we compute the correlations between the leading 250hPa subseasonal V-wind REOFs (the associated rotated principal components or RPCs) and subseasonal precipitation and surface temperature using both MERRA and independent observations. Figs 4 and 5 show examples of the correlations for REOF 1 and REOF 4, respectively. Correlations with absolute values greater than 0.27 are significant at the 5% level, based on the Monte Carlo approach described in section 2. The results show, first of all, that MERRA provides very good estimates of both the temperature and precipitation variability, and in the case of the surface temperature provides information over the oceans that is not available from the gridded station observations. These results give us confidence that we can also use MERRA to estimate the forcing of these waves (see next section).

The leading REOF is associated with a very distinctive pattern of precipitation and temperature correlations that alternate in sign, extending across the Eurasian continent north of the jet, with precipitation correlations exceeded 0.3 in magnitude, while the magnitudes of the temperature correlations exceed 0.6 (Fig. 4). It is noteworthy that there are also significant precipitation correlations (exceeding 0.3) south of the Asian jet, and significant temperature correlations over central China and parts of Northern Africa. The correlations associated with the fourth REOF (Fig. 5) are strongest over North America, with the largest precipitation correlations occurring in the US northern Great Plains extending north into Canada. The temperature correlations have an east-west dipole with one pole centered over the Northern Great Plains and the other over eastern North America. The other leading REOFs also show significant temperature and precipitation

correlations (not shown). REOF 2 is associated with a north/south wet/dry dipole over the U.S. and Canada, and an east/west dipole in temperature in the western and central United States. REOF 3 has significant temperature and precipitation correlations over eastern North America and Europe, and REOF 5 has significant precipitation and temperature correlations extending south and east from the Caspian Sea to India, parts of China, and Indonesia. While the details of the mechanisms by which the upper tropospheric waves impact the surface meteorology are beyond the scope of this paper, we note that the vertical structure of the waves (as determined from correlations with the V-wind at 850mb – not shown) is largely barotropic, although there is some tendency for a westward tilt with height.

The impact of the leading REOFs on surface meteorology is summarized in Figure 6 in terms of an explained variance based on a linear regression that uses the first ten 250hPa V-wind REOFs as predictors. Shaded values are significant at the 5% (10%) level for surface temperature (precipitation) based on the Monte Carlo approach (see section 2). In the case of surface temperature, the REOFs explain more than 60% of the monthly mean subseasonal variance over parts of northern Europe, Russia, and the western United States. In the case of precipitation, the explained variance is somewhat nosier and lower, although there are substantial regions in the North Atlantic, Europe, Russian, southern Eurasia, the North Pacific, and the US and Canada where the explained variance exceeds 30%.

We next examine the time history of the RPCs to get a better sense of the character of the variability, and to determine whether there are particular climate extremes that can be associated with one or more of the leading REOFs. Figure 7 (left panel) shows the 5 leading subseasonal

RPCs for JJA of each year. The subseasonal variability shows little month-to-month persistence, although there is some tendency for extreme anomalies of one sign to be followed by a reversal in sign the following month- a result that is expected since the anomalies over a season must add to zero by design. Examples of extreme occurrences of the leading RPCs include the months of June and July of 2003 (RPC 1), June 1998 (RPC 2), and June 1988 (RPC 4). These are associated with the 2003 European heat wave, the spring/early summer 1998 flooding in the Midwest and northeast and drought to the south, and the 1988 US summer drought. It is noteworthy that the extremes tend to occur in June – something that we will discuss in the next section.

Of course any particular monthly mean anomaly is potentially composed of both intraseasonal and interannual components as quantified in (1). We examine this here by projecting the seasonal mean anomalies onto the subseasonal REOFs. The results (middle panels of Fig. 7) show that the leading subseasonal REOFs do at times have a substantial seasonal mean component, so that the total monthly variance associated with each REOF (right panels of Fig. 7) exhibits considerable month-to-month persistence during some summers. A key example is the summer of 1993 when REOF 4 has a (positive) seasonal mean that dominates the total variance (Figure 7 - second row from bottom), so that the seasonal peak in July during the most intense flooding over the central United States, is a relatively smaller subseasonal fluctuation on top of the seasonal mean. This is in contrast with the summer of 1988, when REOF 4 has a relatively small seasonal mean component, and is instead characterized by a large subseasonal component dominated by a negative event during June of that year at the height of the drought.

We also see that the summer of 2003 was characterized by largely subseasonal variations in RPC 1 (top row of Fig. 7), in which the associated stationary Rossby wave changed sign from negative in June to positive in July, and then back to negative in August. This reflects the subseasonal fluctuations in the 2003 heat wave over Europe, with the most intense heat occurring during June and early August, with a temporary relaxation of the heat wave during July (consistent with our expectations of the impact of REOF 1 on surface temperature shown in Fig. 4). In contrast, the 2010 heat wave over Russia is associated with a positive occurrence of REOF 1 that has a significant seasonal mean component, on top of a large-amplitude positive event that occurred during July - the peak of the Russian heat wave. This is again consistent with our expectations of the impact of REOF 1 on Russian surface temperature (Fig. 4).

Other noteworthy aspects of Fig. 7 include the large positive seasonal mean component of REOF 3 during 2009 associated with a very cool and wet summer extending from the Great Plains to the northeastern United States, and a large negative occurrence of RPC 2 in June 2005, associated with very dry condition over Texas and record June rainfall in North Dakota. While there is no clear evidence of any trends in the seasonal means, there do appear to be extended periods where the REOFs have loadings of the same sign (e.g., REOFs 1 and 2 – top two middle panels). There also appears to be a tendency towards more negative values in the loadings of REOF 5 after the mid 1990s (bottom middle panel of Fig. 7), though this is small compared to the month-to-month subseasonal variability.

Figs. 8 -10 provide examples of the important contributions made by the first and fourth REOFs to the monthly climate anomalies over Eurasia and North America. Here we have selected

several years that have a substantial contribution from REOF 1 based on the RPC loadings shown in Fig 7. The signature of REOF 1 is clearly evident in the v250mb anomalies (Fig. 8), with alternating positive and negative 250mb V-wind anomalies extending across northern Eurasia. It is again noteworthy that most of the large anomalies occur during June. The 2010 anomaly stands out because it occurs during July, and because it has a large seasonal mean component. That month is also distinguished by a large amplitude southern track (embedded within the Asian jet wave guide) of the anomalies – in fact that aspect of the wave is associated with a large negative loading of REOF 5 (bottom right panel of Fig. 7).

Fig. 9 shows the associated surface temperature anomalies. The anomalies are consistent with the signature of REOF 1 (cf. Fig. 5 top panels). The alternating cold and warm surface temperature anomalies reflect the upper level wind and associated height anomalies (with e.g. upper level ridges associated with warm surface conditions over northern Eurasia). Particularly noteworthy are the warm anomalies over Europe during June 2003, and over eastern Russia during July 2010. Also during 2010, the southern track of the 250mb v-wind anomalies (Fig. 8) appears to be associated with cold (and wet – not shown) anomalies over northern Pakistan (also a signature of REOF 1 – Fig. 4), which may have contributed to the intense flooding in that region in July and August. We note that REOF 5 also impacts that region, with the positive phase producing positive rainfall anomalies. In 2010, REOF 5 was negative in the early summer (associated with negative precipitation anomalies) and then switched to positive values in August – presumably contributing to the flooding during that month.

Fig. 10 shows the 250hPa v-wind anomalies during the height of the July 1993 flooding and June 1988 drought over the United States and Canada. Also shown are the associated precipitation and surface temperature anomalies. The signature of REOF 4 is clearly evident in the 250 hPa V-wind anomalies during both months (positive in 1993, and negative in 1988). The precipitation and surface temperature anomalies during 1993 also have a clear signature of REOF 4 (cf. Fig. 5). In the case of the 1988 drought, the precipitation and surface temperature anomalies again show some signature of REOF 4, however, the anomalies are more wide spread, consistent with an important contribution from land feedbacks as suggested by previous studies (e.g., Namias 1991; Atlas et al. 1993). In fact, Dirmeyer and Brubaker (1999) showed that while recycling reaches its maximum during the June peak of the 1988 drought, during the height of the 1993 floods in July, the recycling was considerably lower than during other months.

We next turn to a stationary wave model to try to get a better understanding of the forcing and variability of the wave structures associated with the leading REOFs.

4. Results from Stationary Wave Model Experiments

The stationary wave model (SWM) used in this study is the dry dynamical core of a full nonlinear time-dependent AGCM (Ting and Yu 1998). It is based on the 3-dimensional primitive equations in σ coordinates. The model-generated transient disturbances are suppressed by strong damping. The model has rhomboidal wavenumber-30 truncation in the horizontal and 14 unevenly spaced σ levels in the vertical (R30L14). The SWM has been shown to be a

valuable tool to diagnose the maintenance of both climatological and anomalous atmospheric circulation by evaluating the relative roles of stationary wave forcing over specific regions (e.g., Ting et al. 2001; Held et al. 2002; Lau et al. 2004). More details of the SWM can be found in Ting and Yu (1998).

In the experiments performed here, the background state for the SWM consists of the full three-dimensional climatological JJA flow computed from MERRA for the period 1979-2010. The stationary wave forcing consists of diabatic heating and transient flux convergences that are specified as idealized local forcing functions or estimated from MERRA daily output. We turn first to the idealized forcing experiments.

a) Responses to idealized forcing

The horizontal scales of the idealized diabatic heating and transient vorticity forcing are 40° longitude by 10°latitude, and 10°longitude by 10°latitude, respectively. The vertical profiles of the idealized heating and transient vorticity forcing are defined following Figure 13 of Liu et al (1998). The heating profile has a maximum of 3°K/day in the middle troposphere, and the profile of the transient vorticity forcing has a maximum of $5.6 \times e^{-10}$ sec^{-1} in the upper troposphere.

Figure 11 shows some examples of the response to idealized vorticity sources in selected locations. In the left panels the source is located just east of Japan. The response shows the development of a wave train embedded in the jet that extends eastward into North America. The

wave train becomes fully developed with a zonal wave number 6 structure in about 30 days, and resembles some of the wave trains found in MERRA (cf. REOF 2 in Fig 3). The middle panels of Fig. 11 show another example in which the source is placed in the eastern Pacific just south of the jet. In this case, the wave extends across North America and the Atlantic into Europe, and is again largely embedded in the jet (cf. REOF 4 in Fig. 3). The panels on the right of Fig. 11 show an example where the source is placed slightly to the south of the North Atlantic jet exit region. In this case, the wave activity splits as it moves east over Eurasia, with one branch moving north of the jet across Russia, while the other branch moves slightly south and remains largely embedded in the jet. The basic structure of this wave is quite similar to that of ROEF 1 (Fig. 3)

The above results are generally consistent with previous theoretical studies of boreal summer Rossby waves in the atmosphere. For example, Ambrizzi et al. (1995) summarized the boreal summer wave-guides and preferred propagation patterns towards and away from the wave-guides (e.g. their Fig. 17). The current results are generally consistent with the structures and wave paths found in that study, although the propagation of wave activity over Russia (found in the SWM and MERRA) is less prominent in their study.

We next address the forcing of the leading patterns (REOFs) found in MERRA within the context of the SWM. We begin by carrying out a series of forcing experiments using the idealized heating and vorticity sources described earlier. In one set, we introduce heat sources centered at every 10° longitude and 5° latitude to build up a collection of responses to heating over the Northern Hemisphere. In another set, we build up a collection of responses to vorticity sources over the Northern Hemisphere. Inner products are then formed between each of the

upper level eddy V responses and each of the 5 leading REOFs, and plotted at the forcing location. The result (Fig. 12) gives an indication of those locations where forcing tends to produce a response that resembles one of the REOFs. We interpret the inner product patterns as the optimal forcing distributions for the REOFs. For example, the top panels of Fig. 12 show that heating over Europe generates a response that projects strongly onto REOF1, while heating over Russia (near 60°E) also produces a relatively strong response in REOF 1 but with opposite sign. In addition to forcing that is collocated with the region where the mature wave amplitude is largest, upstream heating along the southern part of the North American/Atlantic jet extending southeastward over Northern Africa also produces a response that projects onto REOF 1. Similar results are obtained for the response to vorticity sources (right top panel in Fig. 12), although the forcing and response tend to be in quadrature.

The next set of panels (second from the top) in Fig. 12 shows that REOF 2 can be forced with heating or vorticity sources anywhere from Europe to western North America along the Asian/Pacific jet. The largest response in REOF 2 to heating occurs just off the west coast of North America, while the strongest response to vorticity forcing occurs just south of the jet in the western Pacific. REOF 3 (third row form the top in Fig. 12) is most readily forced (with both heating and vorticity sources) in a broad region extending from the eastern Pacific just south of the jet, across the United States and Mexico, into the North Atlantic.

REOF 4, in contrast to REOF 3, has a longitudinally more limited region of optimal forcing that is largely confined to the eastern Pacific. As already mentioned in the previous section, REOF 4 played an important role in the US 1988 drought and 1993 flood. The forcing location in the

eastern Pacific is consistent with some of the earlier work on drought in the central United States (e.g., Trenberth and Branstator 1992; Trenberth and Guillemot 1996; Mo et al. 1997). On the other hand, Chen and Newman (1998) suggest that the forcing for the June anomalies lies in the western North Pacific and southeast Asia – a period (early spring) that is particularly conducive to cross-Pacific propagation of Rossby waves as discussed in Newman and Sardeshmukh (1998). They showed that the most sensitive area of forcing for producing a large response over the United States shifts from the east Pacific in late winter to the west Pacific by late spring, and that the amplitude of the forced response can potentially be larger in June than any other month of the year. Our experiments with different basic states (not shown) also show that the June base state produces more robust wave propagation (compared with May and July) across the Pacific in response to forcing in the subtropical western Pacific. Nevertheless, the pattern most relevant to the 1988 drought (REOF 3) is in our case more easily forced in the eastern North Pacific. We do find prior to the development of REOF 4 in late May/early June, there is evidence for Rossby wave propagation across the Pacific during the first half of May that could set the stage (e.g., provide the vorticity forcing in the eastern Pacific) for the development of REOF 4 later that month. Finally, REOF 5 (bottom panels of Fig. 12) is most readily forced by heating in a region centered on 45°N and 55°E (just east of the Caspian Sea), and by vorticity sources just to the northwest of that region.

The optimal forcing patterns suggest that there are preferred regions of "upstream" forcing that might serve to initiate the waves. Other inferred forcing regions that are basically in phase with the regions of the largest wave response could potentially represent regions where local feedbacks are important for maintaining the wave. An example is REOF 1, where one could

argue that while the wave could be initiated by (say vorticity) forcing somewhere upstream of the wave along the North Atlantic jet, once the wave is mature, local heating feedbacks over Eurasia could play an important role in helping to maintain the wave (e.g., Fischer et al. 2007). This is in contrast with REOF 4 where the primary forcing seems to be upstream of the wave over the eastern Pacific.

b) Response to Forcing Estimated from MERRA

Ting and Yu (1998) develop the equations for the nonlinear anomaly model that form the basis of the stationary wave model used here. The prognostic variables (vorticity, divergence, temperature, and log-surface pressure) are departures from the prescribed basic state (in our case the JJA mean from MERRA). The time mean quadratic transient terms act as forcing terms in each of the prognostic equations. Following Wang and Ting (1999), the leading terms of the forcing are estimated from 3-hourly MERRA output on pressure levels as:

$$TF_{vor} = -\nabla \cdot \left(\overline{V' \zeta'} \right), \tag{2a}$$

$$TF_{div} = k \cdot \nabla \times \left(\overline{V' \xi'} \right) - \frac{1}{2} \nabla^2 \left(\overline{V' \cdot V'} \right), \tag{2b}$$

$$TF_{temp} = -\left(\frac{p}{p_o} \right)^{R/c_p} \left(\nabla \cdot \left(\overline{V' \theta'} \right) + \frac{\partial \left(\overline{\omega' \theta'} \right)}{\partial p} \right), \tag{2c}$$

where ζ is the vorticity, ρ is the divergence, V is the horizontal wind, p is pressure, ω is the pressure vertical velocity, and TF_{vor}, TF_{div}, and TF_{temp} indicate that these are the transient forcing terms in the vorticity, divergence and temperature equations, respectively. The overbar indicates a monthly mean, and the prime indicates a deviation from the monthly mean. The full form of the transient forcing terms can be found in Ting and Yu (1998). Also following Wang and Ting (1999), the total diabatic heating is estimated from MERRA as a residual of the temperature equations as:

$$\bar{Q} = \frac{\partial \bar{T}}{\partial t} + \bar{V} \cdot \nabla \bar{T} + \bar{\omega}\left(\frac{\partial \bar{T}}{\partial p} - \frac{R\bar{T}}{c_p p}\right) - TF_{temp}. \qquad (3)$$

The above stationary wave forcings are then linearly interpolated onto the R30L14 resolution of the SWM. In order to examine the forcing associated with the REOFs, we compute the forcing at each grid point and for each summer month based on daily MERRA data for 1979-2010. The subseasonal monthly transient forcing and diabatic heating are then regressed against the normalized monthly subseasonal RPCs.

The results of the regression for the 5 leading REOFs are shown in Fig. 13 for the vertically integrated diabatic heating (left panels) and the vorticity transients in the upper troposphere (right panels). The vertically-integrated heating fields (left panels) to a large extent resemble the correlations with the precipitation (e.g., Figs. 4 and 5). This is not surprising, and reflects the difficulties of separating the initial forcing from the response and feedbacks associated with the mature wave. The estimated eddy transient vorticity forcing[3] is shown in the right panels for the upper troposphere. The fields are very noisy and for display purposes, have been smoothed by applying an inverse Laplacian operator. Again, the fields reflect the basic structures of the mature waves, although there is some suggestion that they reflect aspects of the idealized "optimal" forcing structures show in Fig. 12 (right panels). For example, the forcing along the North Atlantic jet and over Europe, and the forcing over the eastern North Pacific resemble the optimal forcing structures in those regions for REOF1 and REOF 2, respectively. In any event, we can assess the accuracy of the estimated forcing by using it to force the stationary wave model, and determining whether it reproduces the REOFs.

Fig. 14 shows the results of forcing the SWM with the above 3-dimensional diabatic heating and transient eddy fields associated with the 5 leading REOFs as determined from the linear regression. The strength of the forcing is set by assuming an amplitude of one standard deviation in the predictors (the RPCs). The response to the transient divergence forcing is small in all cases and is not shown. In fact, the transient vorticity forcing dominates the response in all cases, with weaker contributions from the heating and transient temperature forcing terms. Overall the SWM, when forced with the 3 dimensional forcing terms estimated from MERRA, does a remarkably good job of reproducing the individual REOF structures, although the

[3] The SWM is forced with the transient vorticity forcing with the zonal mean removed (the eddy component).

amplitude is about ½ that expected (the amplitude corresponding to 1 standard deviation of the REOFs). The reasons for this are unclear, though it may be that (2) underestimates the magnitude of the transient forcing terms.

In the case of REOF 1 (left panels of Fig. 14a), the temperature transients also play a significant role, with a response that is in quadrature with the response to the vorticity transients acting to shift the total response somewhat to the west. The heating in the eastern Pacific appears to play a significant role in the REOF 2 response (middle panels of Fig. 14a), although the response is largely out of phase with the response to the vorticity transients. The remaining leading REOFs (3-5) have only minor contributions from all but the transient vorticity forcing term. While overall, the SWM forced with the MERRA transients and heating reproduces the basic structure of the leading REOFs remarkably well, there are some differences – notably the ROEF 5 results (right panels of Fig. 14b) show a much stronger amplitude at high latitudes (near 60°N), than is found in REOF 5. This is also true for the third and fourth REOFs – though less so.

5. Summary and Conclusions

The results of this study show that stationary Rossby waves play an important role in boreal summer subseasonal variability, accounting for more than 30% (60%) of the monthly mean precipitation (surface temperature) variability over many regions of the extratropical land areas, including the US northern Great Plains, parts of Canada, Europe, and Russia. The waves tend to develop within the mean jets and, within a few weeks, span much of the global. A decomposition of the monthly mean 250mb meridional wind variability into REOFs highlights

the regions where the Rossby waves tend to occur. The wave associated with the leading REOF appears to develop in the North Atlantic jet and then splits as it exits the jet, with most of the wave energy propagating north of the Eurasian jet across northern Europe and Russia, where it is a dominant contributor to monthly surface temperature and precipitation variability. The second REOF spans the globe from India to North America, while the third and fourth extend from the eastern Pacific to Europe: all three having important impacts on the hydroclimate of North America. The fifth REOF extends eastward from Europe across southern Eurasia, into the North Pacific.

The waves are at times (either as a subseasonal event or in combination with a seasonal mean component) major contributors to short term climate extremes such as heat waves and flooding events. Examples include the 2003 European and 2010 Russian heat waves (REOF 1), and the June peak of the 1988 drought and the July peak of the 1993 flood over the United States (REOF 4). The significant projection of seasonal mean variability on the subseasonal REOFs is consistent with earlier work (Ding and Wang 2004), which found that stationary Rossby Waves play an important role on interannual time scales in the teleconnections that span from Eurasia to North America.

A stationary wave model, driven by localized heating or vorticity sources and using a climatological three-dimensional JJA base state, is able to reproduce some of the basic characteristics of the waves identified from MERRA. This includes the basic wave structures, wavelengths and their circum global extent. A series of experiments, in which the SWM was forced with localized heating and vorticity sources, quantified the preferred regions of forcing of

the leading REOFs. The forcing patterns are typified by wave-like structures with the largest responses occurring when the forcing is just south of the jets and/or embedded in the developing wave, the latter forcing regions suggest that local feedbacks may be important.

A second set of experiments were carried out in which the SWM model was forced by MERRA-estimates of the heating and transient forcing terms associated with each REOF. The responses to the forcing estimates show a remarkable agreement with the REOFs, indicating that the MERRA estimates of the forcing appear to be realistic. A key result is that the transient vorticity fluxes are by far the dominant forcing terms for the leading REOF wave structures, with heating and temperature transients playing a secondary role.

The largest amplitude waves tend to occur in June. This is consistent with previous findings regarding the seasonality of the Pacific wave guide (Newman and Sardeshmukh 1998). It is, however, not clear that this is also true for the wave guide associated with the Atlantic jet and in particular the development of the Eurasian Rossby wave (REOF 1). Limited tests with the SWM (not shown) do not suggest large sensitivities of the response to forcing in the Atlantic jet to the annual cycle of the summer waveguide. In fact, as the wave energy associated with REOF 1 propagates out of the Atlantic jet exit region and across northern Russia it does so in a region of climatologically weak zonal winds. We have found some evidence, again based on SWM experiments, that an anomalous eastward extension of the Atlantic jet across northern Europe and Russia (such as that found during the months prior to the 2003 and the 2010 heat waves) does facilitate the development of the Eurasian Rossby wave.

While we have shown that stationary Rossby waves play an important role in subseasonal variability, and at times are major players in the development of short term climate extremes, it is as yet unclear to what extent they are predictable at monthly time scales. The important role of vorticity transients in forcing the waves would suggest that the predictability may be limited, though it is not clear the extent to which the slow changes in the jet and associated changes in the wave guides (that could be linked to SST changes) may play a role especially for some of the most extreme events such as the 2003 European or the 2010 Russian heat waves, or periods (e.g., during the 1993 floods) when they seem to contribute to seasonal mean anomalies. In any event, current GCMs appear to be deficient in reproducing aspects of the summer jet climatology that likely limit their ability to accurately simulate and predict the development of such Rossby waves. In addition to improving the models, it is possible that ensemble initialization schemes that take advantage of the identified preferred forcing patterns (e.g., Fig. 12) to better span the forecast uncertainty, could produce greater skill than is achieved in current extended range forecasts.

Acknowledgements: Support for this project was provided by the NASA Modeling, Analysis and Prediction (MAP) Program, and the NOAA Climate Prediction Program for the Americas (CPPA).

References

Adler, R.F., G.J. Huffman, A. Chang, R. Ferraro, P. Xie, J. Janowiak, B. Rudolf, U. Schneider, S. Curtis, D. Bolvin, A. Gruber, J. Susskind, P. Arkin, 2003: The Version 2 Global Precipitation Climatology Project (GPCP) Monthly Precipitation Analysis (1979-Present). J. Hydrometeor., 4,1147-1167.

Ambrizzi, T., B. J. Hoskins, and H.-H. Hsu, 1995: Rossby wave propagation and teleconnection patterns in the austral winter. *J. Atmos. Sci.,* **52,** 3661–3672.

Atlas, R., N. Wolfson, and J. Terry. 1993. The effect of SST and soil moisture anomalies on GLA model simulations of the 1988 U.S. summer drought. J. Climate 6:2034–2048.

Bloom, S., L. Takacs, A. DaSilva, and D. Ledvina, 1996: Data assimilation using incremental analysis updates. *Mon. Wea. Rev.*, **124**, 1256-1271.

Branstator, G., 2002: Circumglobal teleconnections, the jet stream waveguide, and the North Atlantic Oscillation. *J. Climate,* **15,** 1893–1910.

Carril, A. F., S. Gualdi, A. Cherchi and A. Navarra, 2007: Heatwaves in Europe: areas of homogeneous variability and links with the regional to large-scale atmospheric and SSTs anomalies. Climate Dynamics, 10.1007/s00382-007-0274-5

Chen, P. and M. Newman, 1998: Rossby-wave propagation and the rapid development of upper-level anomalous anticyclones during the 1988 U.S. drought. *J. Climate*, **11**, 2491-2504

Ding, Q., and B. Wang, 2005: Circumglobal Teleconnection in the Northern Hemisphere Summer. *J. Climate*, **18**, 3483-3505.

Dirmeyer, P. A. and Brubaker, K. L., 1999: Contrasting evaporative moisture sources during the drought of 1988 and the flood of 1993, J. Geophys. Res., 104(D16), 19383–19397.

Fischer, E. M., S. I. Seneviratne, P. L. Vidale, D. Lüthi, C. Schär, 2007: Soil Moisture–Atmosphere Interactions during the 2003 European Summer Heat Wave. *J. Climate*, **20**, 5081–5099. doi: 10.1175/JCLI4288.1

Held, I. M., M. Ting, and H. Wang, 2002: Northern winter stationary waves: theory and modeling. *J. Climate*, **15**, 2125-2144.

Hoskins, B.J., and T. Ambrizzi, 1993: Rossby wave propagation on a realistic longitudinally varying flow. *J. Atmos. Sci.,* **50,** 1661– 1671

Koster R.D., M.J. Suarez, M. Heiser, 2000: Variance and predictability of precipitation at seasonal-to-interannual timescales. J. Hydrometeor., 1, 26-46.

Lau, K-M. and H-Y. Weng, 2002: Recurrent teleconnection patterns linking summertime precipitation variability over east Asia and North America. *J. Meteor. Soc. Japan*, **80**:1309–1324

Lau, K-M., K.-M. Kim, and J.-Y. Lee, 2004: Interannual variability, global teleconnection and potential predictability associated with the Asian summer monsoon. *East Asian Monsoon*, C. P. Chang, Ed., World Scientific, 564 pp.

Liu, Alan Z., Mingfang Ting, Hailan Wang, 1998: Maintenance of Circulation Anomalies during the 1988 Drought and 1993 Floods over the United States. *J. Atmos. Sci.*, **55**, 2810–2832.

Lyon, B., and R.M. Dole, 1995: A diagnostic comparison of the 1980 and 1988 U. S. summer heat wave-droughts. *J. Climate*, **8**, 1658–1675.

Mitchell T.D. and Jones P.D. 2005: An improved method of constructing a database of monthly climate observations and associated high-resolution grids. *Int. J. Climatol*., **25**, 693–712.

Mo, K.C., J.N. Paegle, and R.W. Higgins, 1997: Atmospheric Processes Associated with Summer Floods and Droughts in the Central United States. J. Climate, 10, 3028–3046.

Namias, J., 1983: Some causes of United States drought. *J. Appl. Meteor.*, **22**, 30–39.

_____, 1991: Spring and summer 1988 drought over the contiguous United States—causes and prediction. *J. Climate*, **4**, 54–65.

Newman, M., and P.D. Sardeshmukh, 1998: The impact of the annual cycle on the North Pacific/North American response to remote low-frequency forcing. *J. Atmos. Sci.*, **55**, 1336-1353.

Oppenheim, A., V. and R. W. Schafer, 1975: Digital Signal Processing, Prentice-Hall, Inc., Engleweek Cliffs, New Jersey. pp 585.

Parker, M. D. and R. H. Johnson, 2000: Organizational modes of midlatitude mesoscale convective systems. *Mon. Wea. Rev*, **128**:3413–3436.

Richman M.B., 1986. Rotation of principal components. J. Climatol., 6, 293–335.

Rienecker, M.M., M.J. Suarez, R. Todling, J. Bacmeister, L. Takacs, H.-C. Liu, W. Gu, M. Sienkiewicz, R.D. Koster, R. Gelaro, I. Stajner, and E. Nielsen, 2008: *The GEOS-5 Data Assimilation System- Documentation of Versions 5.0.1, 5.1.0, and 5.2.0*. Technical Report Series on Global Modeling and Data Assimilation, NASA/TM-2007-104606, M.J. Suarez, Ed., Vol. 27, 95 pp.

Rienecker M.M., and coauthors, 2011. MERRA - NASA's Modern-Era Retrospective Analysis for Research and Applications. *J. Climate* (this issue).

Richman M.B., 1986. Rotation of principal components. J. Climatol., 6, 293–335.

Ting, M. and L. Yu, 1998: Steady response to tropical heating in wavy linear and nonlinear baroclinic models. *J. Atmos. Sci.,* **55**, 3565–3582.

Ting, M. F., H. L. Wang and L. H. Yu, 2001: Nonlinear stationary wave maintenance and seasonal cycle in the GFDL R30 GCM. *J. Atmos. Sci.*, **58**, 2331-2354.

Trenberth, K.E. and G. W. Branstator, 1992: Issues in establishing causes of the 1988 drought over North America. *J. Climate,* **5,** 159–172.

Trenberth, K.E. and C.J. Guillemot, 1996: Physical processes involved in the 1988 drought and 1993 floods in North America. J. Climate, 9, 1288-1298.

Wang, Shih-Yu & Lawrence E. Hipps & Robert R. Gillies & Xianan Jiang & Alan L. Moller, 2009: Circumglobal teleconnection and early summer rainfall in the US Intermountain West. Theor Appl Climatol DOI 10.1007/s00704-010-0260-4.

Wang, Hailan, Mingfang Ting, 1999: Seasonal Cycle of the Climatological Stationary Waves in the NCEP–NCAR Reanalysis. *J. Atmos. Sci.*, **56**, 3892–3919.

List of Figures

Absolute values exceeding 0.27 are significant at the 5% level based on a Monte Carlo test (see text).

Figure 5: Same as Figure 4 but for REOF4.

Figure 6: The spatial distribution of the fraction of monthly (JJA-1979-2010) subseasonal variance of surface air temperature (top panel) and precipitation (bottom panel) explained by the first ten 250mb subseasonal v-wind REOFs, based on a linear regression. Contours start at 0.3 with a 0.1 interval. Shaded values are significant at the 5% (10%) level for temperature (precipitation) based on a Monte Carlo test (see text).

Figure 7: Left panel: The five leading rotated principle components (RPCs) of the 250mb subseasonal monthly mean v-wind anomalies for JJA of 1979-2010. Middle panel: The projection of the JJA seasonal mean 250mb v-wind anomalies onto the subseasonal REOFs. Right panel: The sum of a) and b), equal to the projection of the full monthly 250mb v-wind anomalies onto the subseasonal REOFs.

Figure 8: The MERRA 250hPa v-wind anomalies (deviations from the 1979-2010 monthly means) for selected months with a large amplitude in REOF 1 (see Fig. 7). REOF 1 had large negative values during June 1979, June 1982, and June 2003. It had large positive values during June 1987, June 1989, and July 2010. Units are m/s. Contours are the long-term mean (1979-2010) monthly 250hPa u-wind at 15, 20, 25 m/s.

Figure 9: Same as Fig. 8, except for the MERRA surface air temperature anomalies. Units are °C.

Figure 10: Top panel: The MERRA 250hPa v-wind anomalies (deviations from the 1979-2010 monthly means) for July 1993. Second from top: The MERRA precipitation (left) and surface air temperature (right) anomalies during July 1993. Third from top: The MERRA 250hPa v-wind anomalies (deviations from the 1979-2010 monthly means) for June 1988. Bottom panels: The MERRA precipitation (left) and surface air temperature (right) anomalies during June 1988. V-wind has units of m/s, precipitation has units of mm/day, and surface air temperature has units of °C.

Figure 11: The time evolution of the response of the eddy v-wind at σ=0.257 to an idealized vorticity source at 150E, 40N (left panels), 220E, 40N (middle panels), and 0E, 50N (right panels). The results are from a stationary wave model with a 3-dimensional JJA mean base state taken from MERRA for the period 1979-2010. See text for details of the forcing. Contour interval is 0.08 m/s.

Figure 12: The optimal forcing regions for the 5 leading REOFs based on the stationary wave model results using a JJA 1979-2010 mean three-dimensional base state from MERRA. The left panels show the optimal patterns for the heating, while the right panels show the optimal patterns for vorticity. The patterns are computed as the inner product between the eddy v-wind response at σ=0.257 to the forcing and the REOFs (see text for details). Units are arbitrary.

Figure 13: Vertically integrated heating (left panels) and eddy (zonal mean removed) transient vorticity forcing at σ=0.257 (right panels) estimated from MERRA associated with each REOF. The results are based on a simple linear regression at each grid point in which the predictor is the REOF and the predictand is the subseasonal forcing. The results are plotted assuming one standard deviation in the RPCs. Units in the left panels are °K/day. The transient vorticity forcing fields are smoothed by applying the inverse Laplacian (units are $m^2\ s^{-2}$).

Fig. 14a: The first row is the subseasonal monthly JJA V250mb v-wind regressed against the three leading REOFs, and plotted assuming one standard deviation in the REOFs. The remaining rows are the responses to the estimated forcing terms for the first (left panels), second (middle panels) and third (right panels) REOFs. The second from the top row is the response to the total forcing. The third row is the response to the heating. The fourth row shows the response to the total (temperature plus vorticity plus divergence) transient forcing. The fifth and sixth rows show the separate responses to the vorticity and temperature transients, respectively. Units: m/s.

Fig. 14b: Same as Fig. 14a, except for the fourth (left panels) and fifth (right panels) leading REOFs.

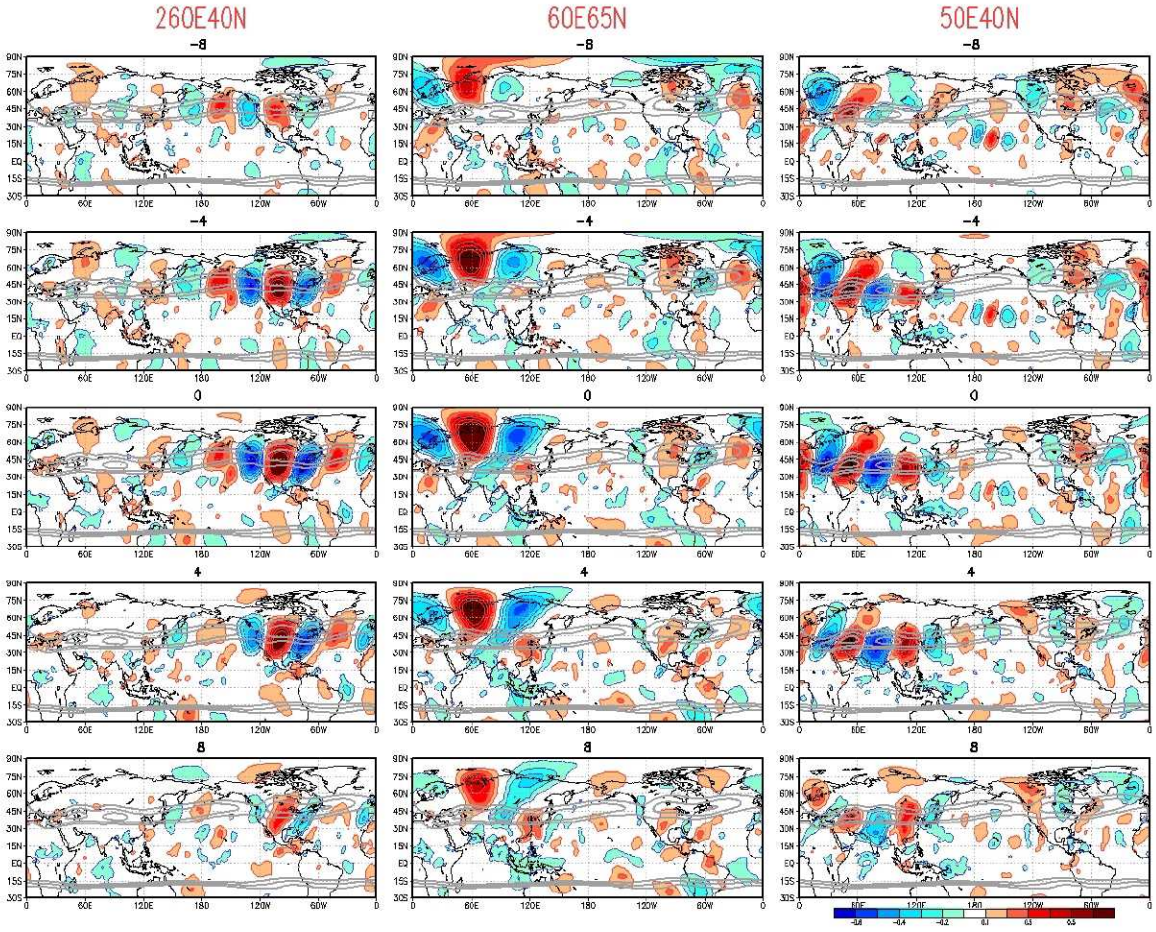

Figure 1: Lag correlations (-8, -4, 0, 4 and 8 days) of the MERRA 30-90 day filtered 250hPa V-wind for JJA of 1979-2010. The correlations are with respect to 250hPa V-wind indices at (260E, 40N - left panels), (60E, 65N - middle panels), and (50E, 40N - right panels). The thick gray contours show the long-term JJA mean (1979-2010) 250hPa u-wind at 15, 20, 25m/s.

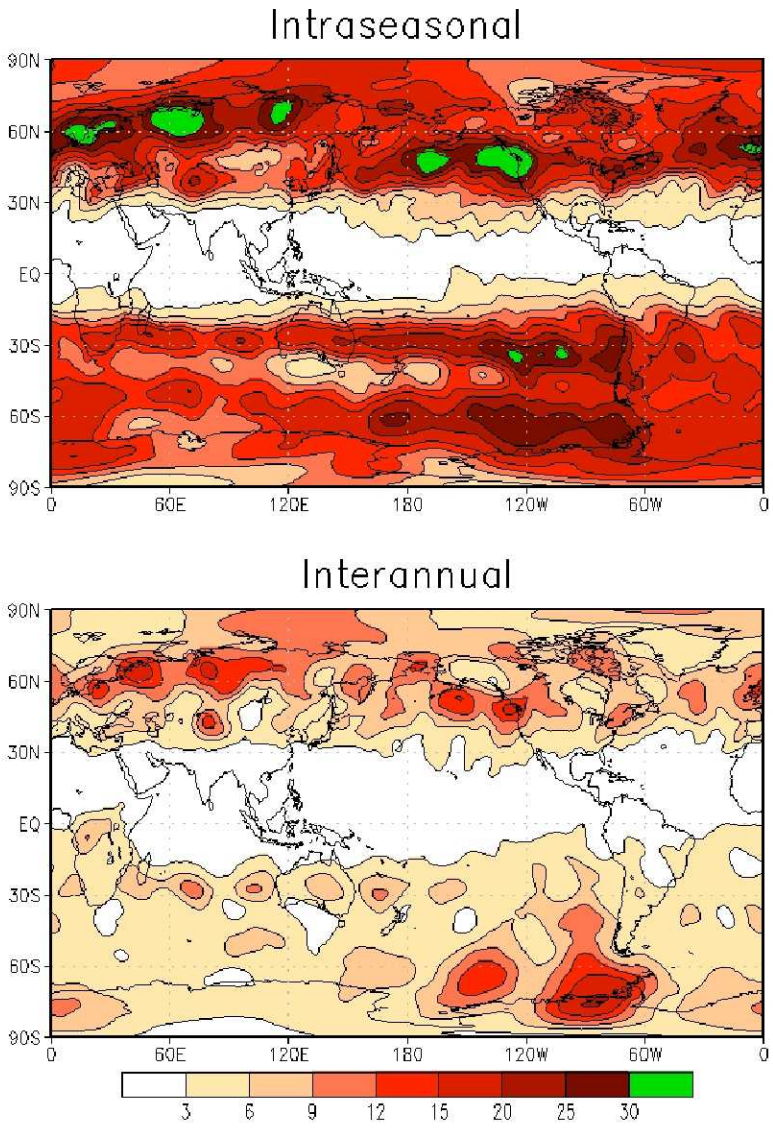

Figure 2: Variance of the monthly mean 250mb V-wind anomalies for JJA for the period 1979-2010. The total seasonal mean monthly variance is decomposed into the intraseasonal variance of monthly means (top panel), and the interannual variance of the seasonal mean anomalies (bottom panel). See text for details. Units are $(m/s)^2$.

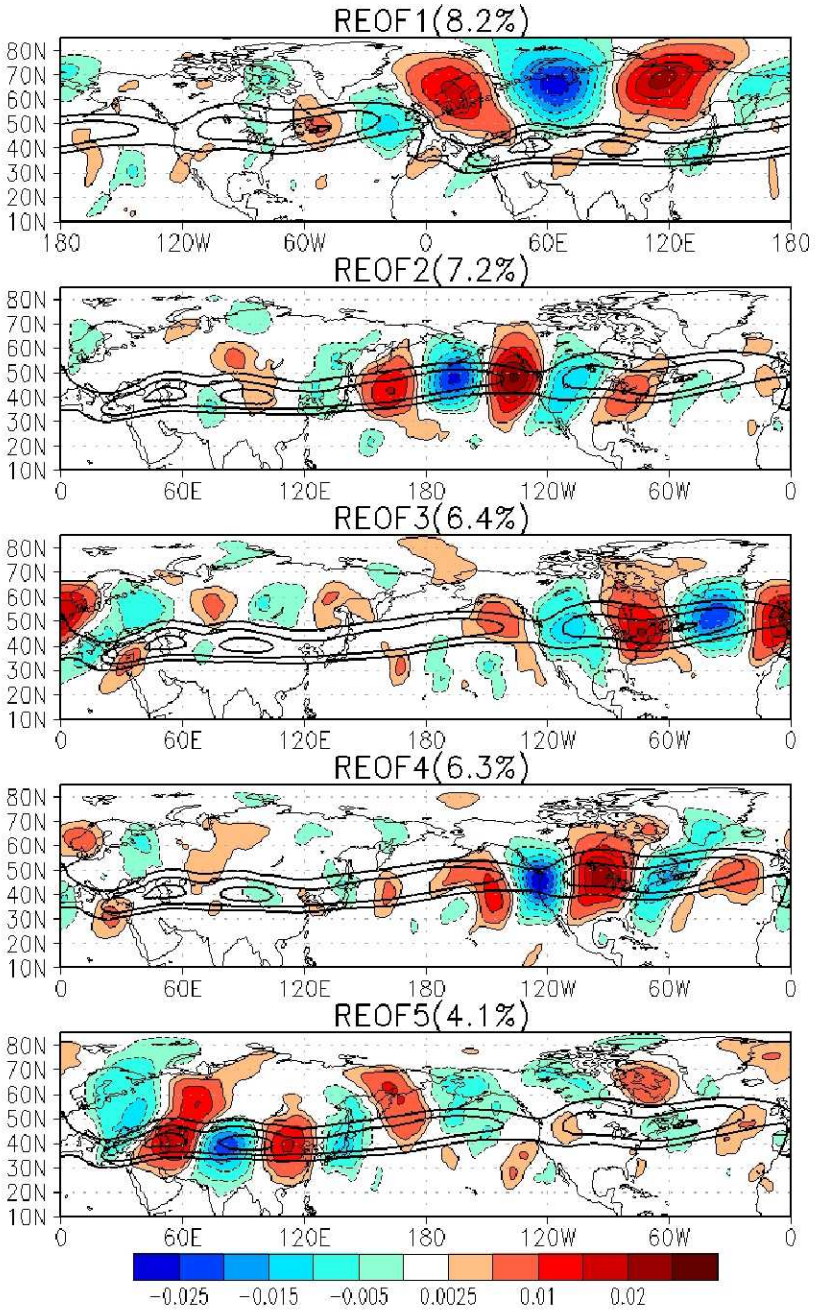

Figure 3: The leading Rotated Empirical Orthogonal Functions (REOFs) of the 250mb intraseasonal monthly mean v-wind anomalies for JJA of 1979-2010. Units are arbitrary. The thick black contours are the long-term JJA mean (1979-2010) 250hPa u-wind at 15, 20, 25m/s.

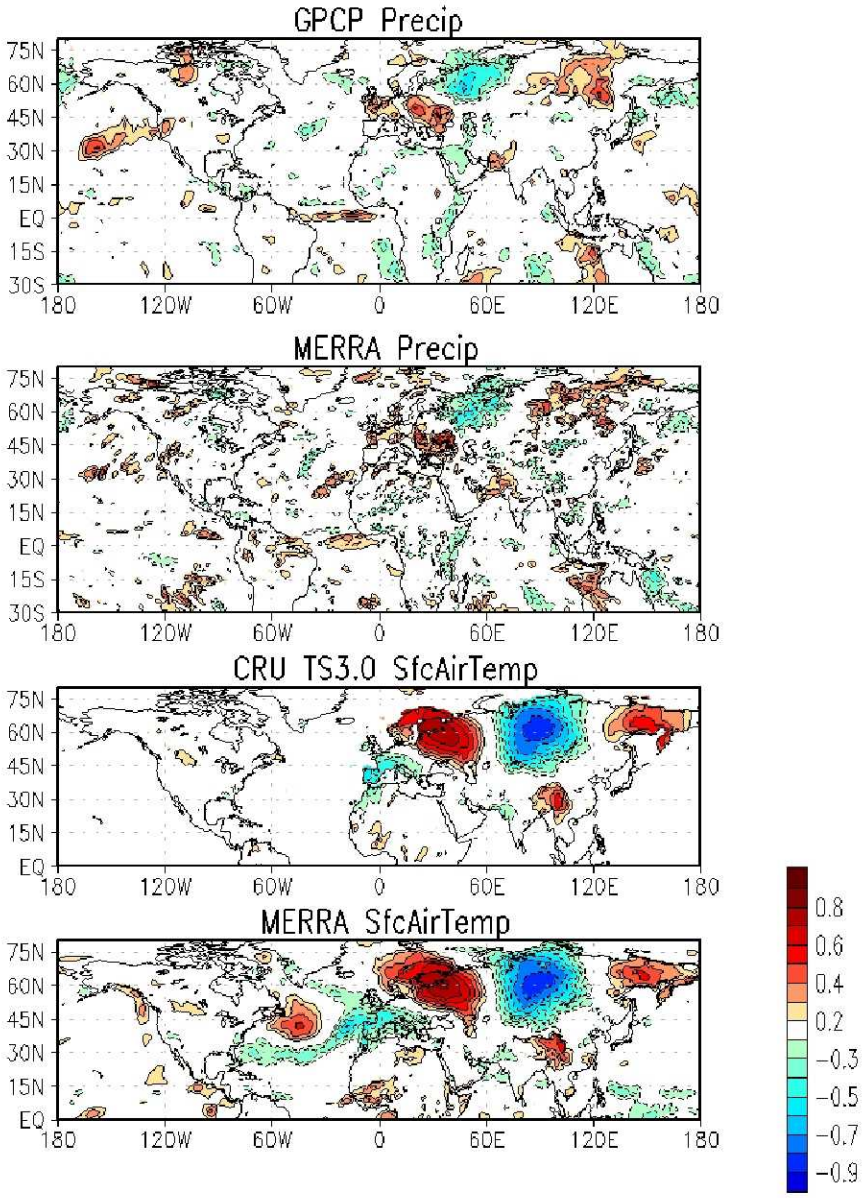

Figure 4: The correlations between the first REOF of the 250mb subseasonal v-wind anomalies and subseasonal a) GPCP precipitation, b) MERRA precipitation, c) CRU TS3.0 surface air temperature, d) MERRA surface air temperature for JJA of 1979-2005. Note that 1979-2005 is the period that all the data are available. The contour interval is 0.1, starting at +/- 0.2. Correlations with absolute values exceeding 0.27 are significant at the 5% level based on a Monte Carlo test (see text).

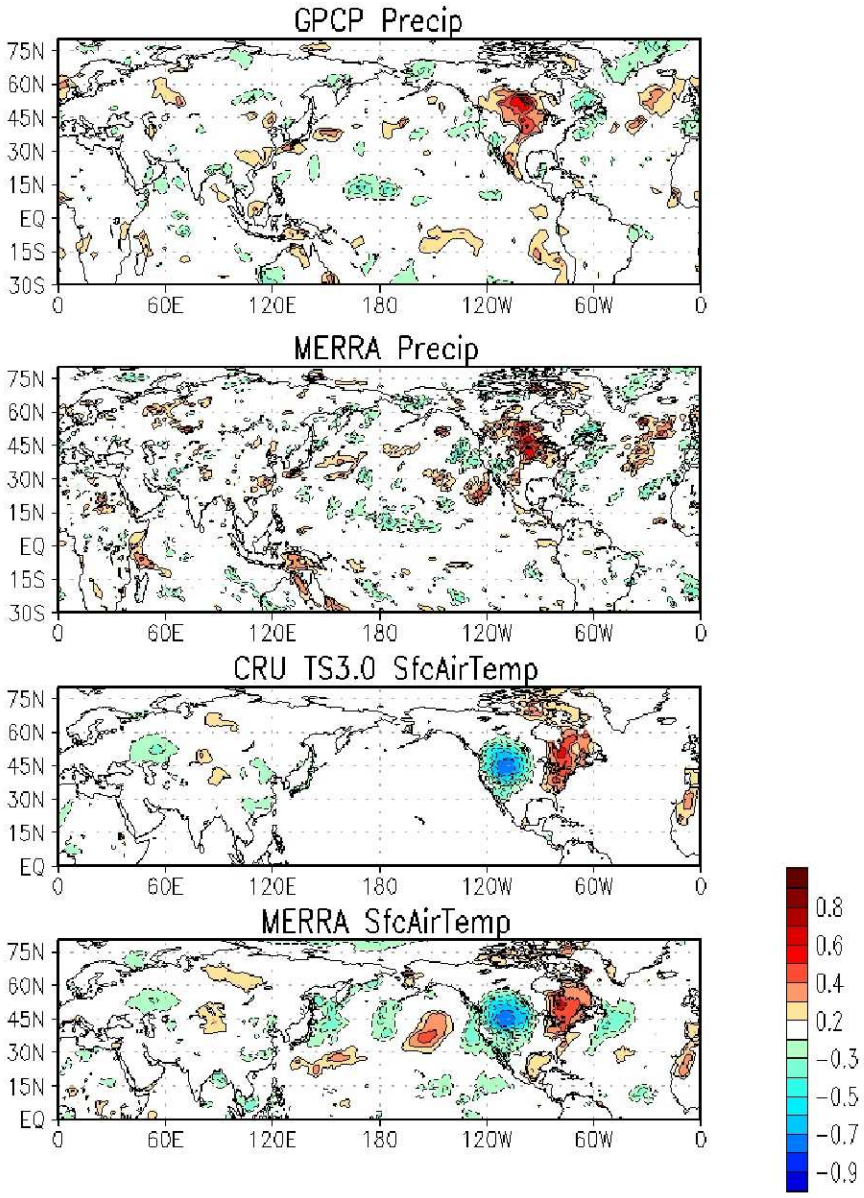

Figure 5: Same as Figure 4 but for REOF4.

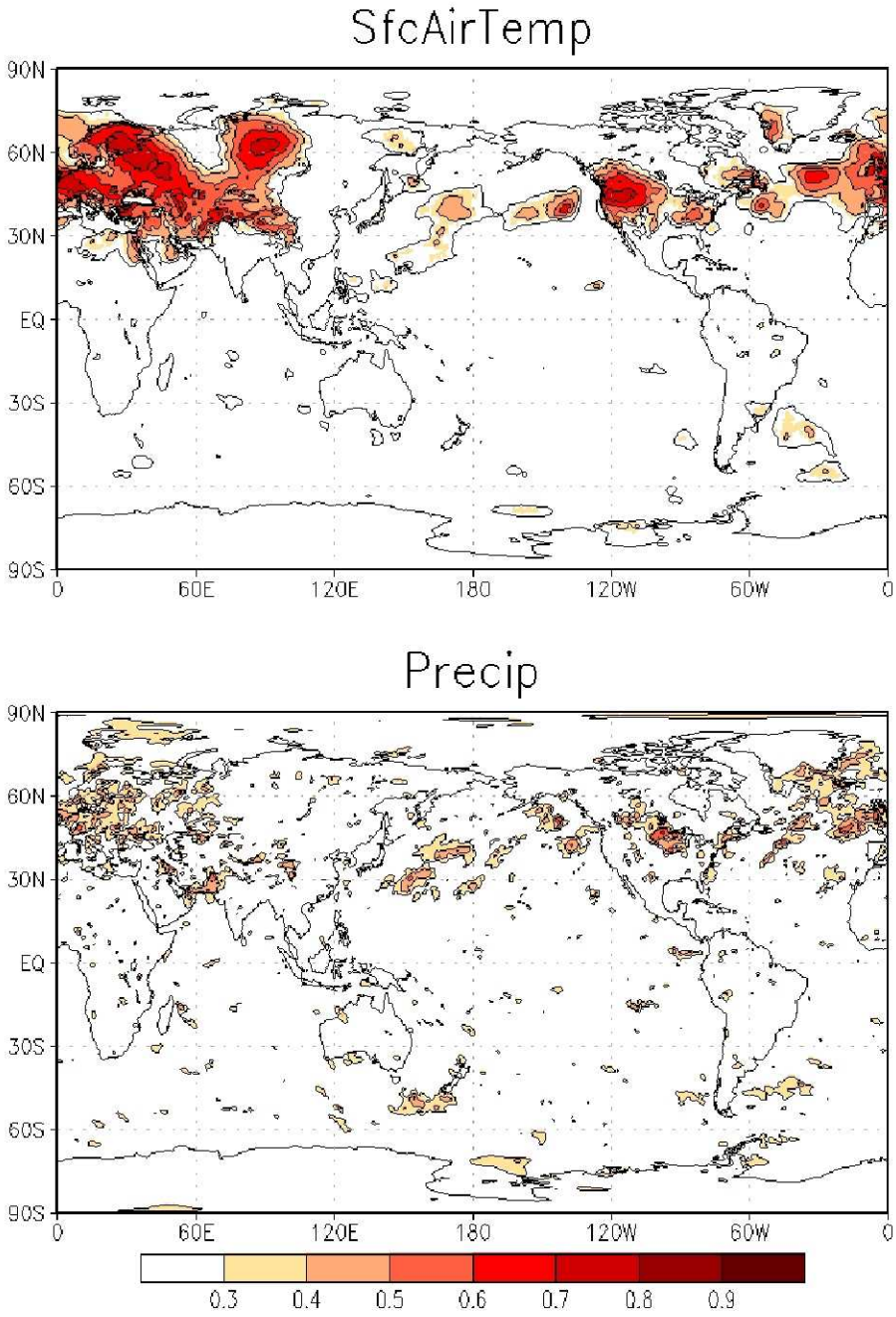

Figure 6: The spatial distribution of the fraction of monthly (JJA-1979-2010) subseasonal variance of surface air temperature (top panel) and precipitation (bottom panel) explained by the first ten 250mb subseasonal v-wind REOFs, based on a linear regression. Contours start at 0.3 with a 0.1 interval. Shaded values are significant at the 5% (10%) level for temperature (precipitation) based on a Monte Carlo test (see text).

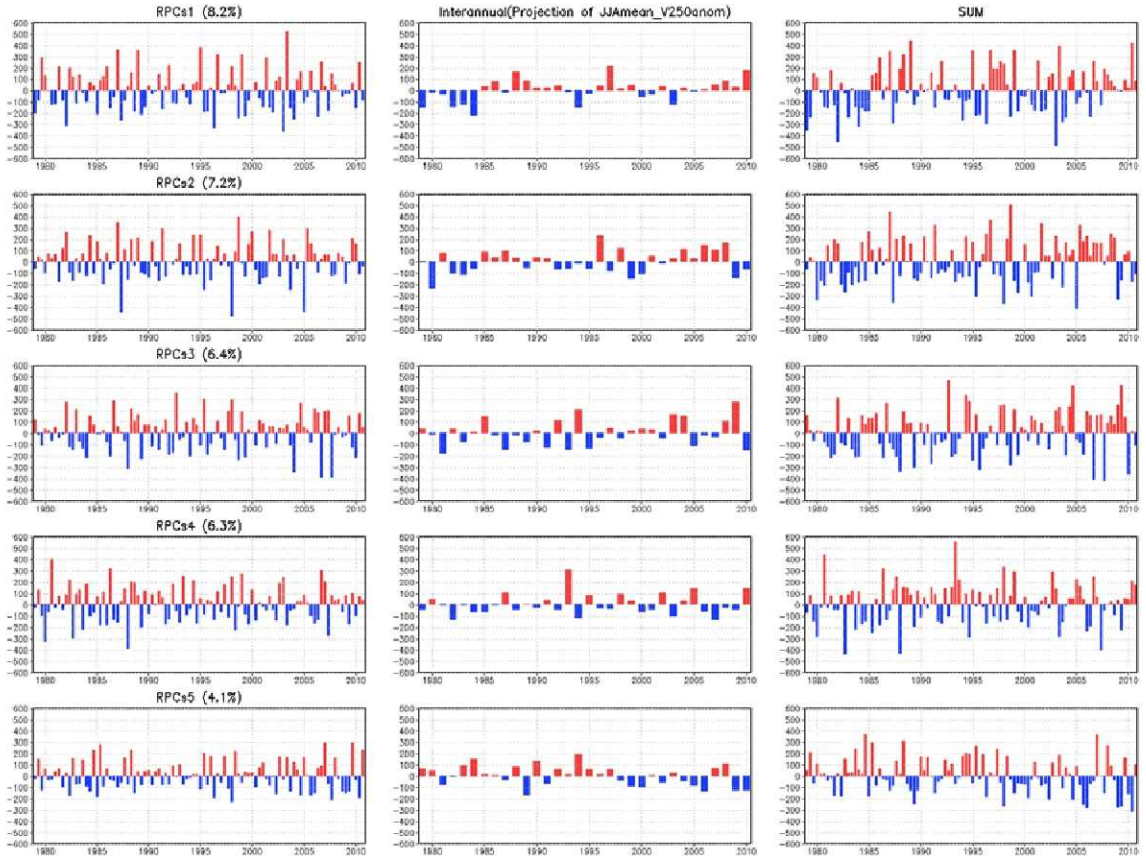

Figure 7: Left panel: The five leading rotated principle components (RPCs) of the 250mb subseasonal monthly mean v-wind anomalies for JJA of 1979-2010. Middle panel: The projection of the JJA seasonal mean 250mb v-wind anomalies onto the subseasonal REOFs. Right panel: The sum of a) and b), equal to the projection of the full monthly 250mb v-wind anomalies onto the subseasonal REOFs.

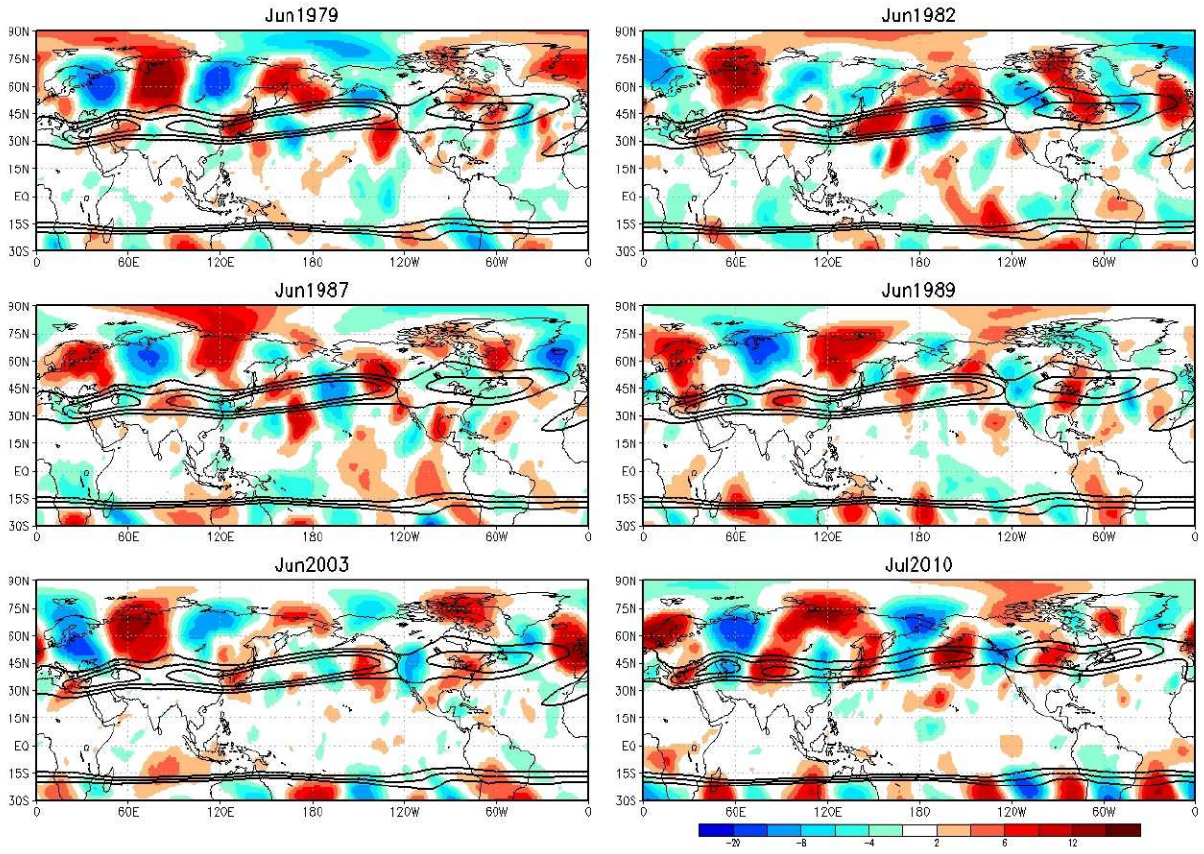

Figure 8: The MERRA 250hPa v-wind anomalies (deviations from the 1979-2010 monthly means) for selected months with a large amplitude in REOF 1 (see Fig. 7). REOF 1 had large negative values during June 1979, June 1982, and June 2003. It had large positive values during June 1987, June 1989, and July 2010. Units are m/s. Contours are the long-term mean (1979-2010) monthly 250hPa u-wind at 15, 20, 25 m/s.

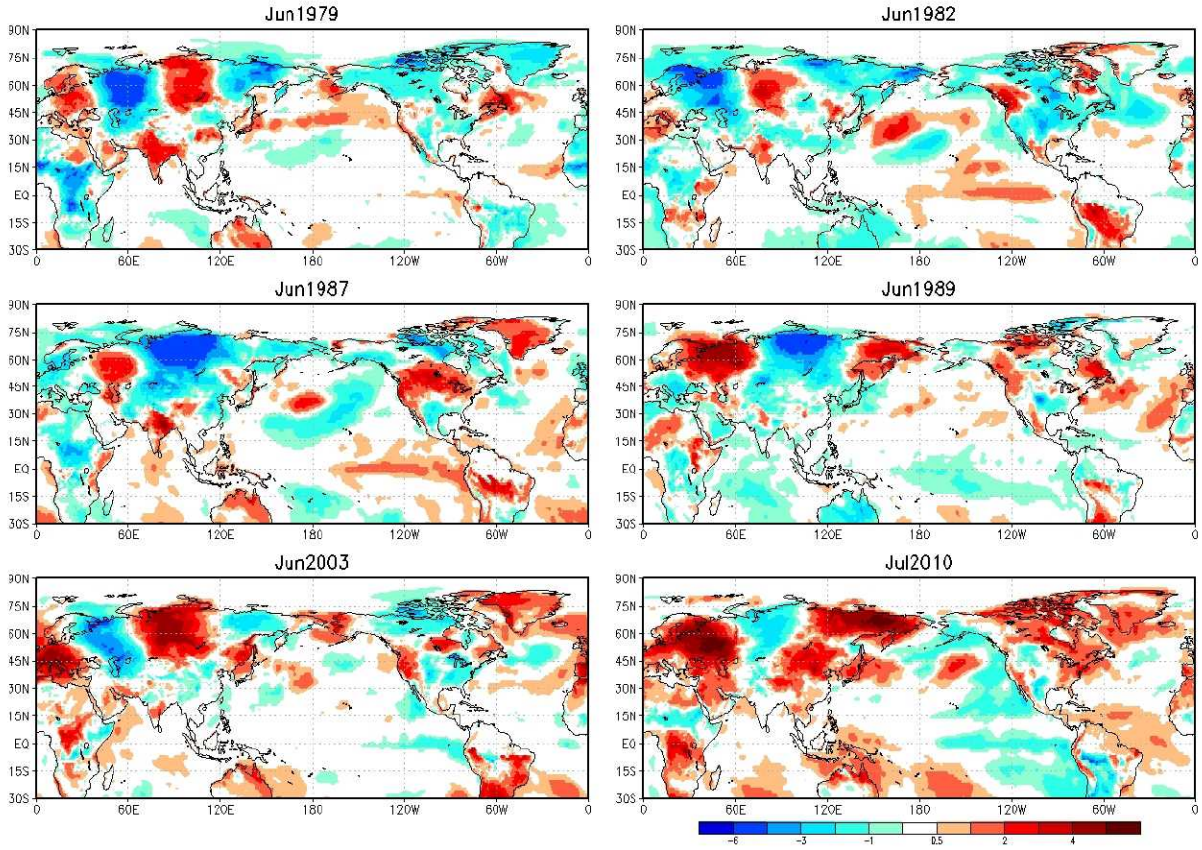

Figure 9: Same as Fig. 8, except for the MERRA surface air temperature anomalies. Units are °C.

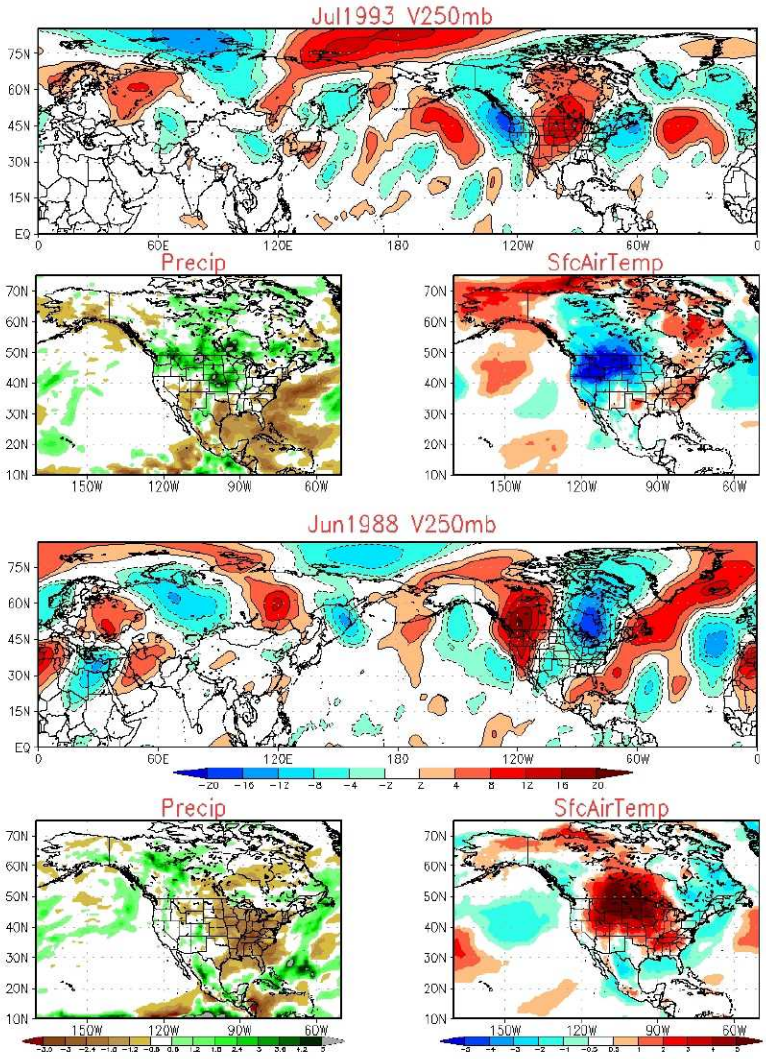

Figure 10: Top panel: The MERRA 250hPa v-wind anomalies (deviations from the 1979-2010 monthly means) for July 1993. Second from top: The MERRA precipitation (left) and surface air temperature (right) anomalies during July 1993. Third from top: The MERRA 250hPa v-wind anomalies (deviations from the 1979-2010 monthly means) for June 1988. Bottom panels: The MERRA precipitation (left) and surface air temperature (right) anomalies during June 1988. V-wind has units of m/s, precipitation has units of mm/day, and surface air temperature has units of °C.

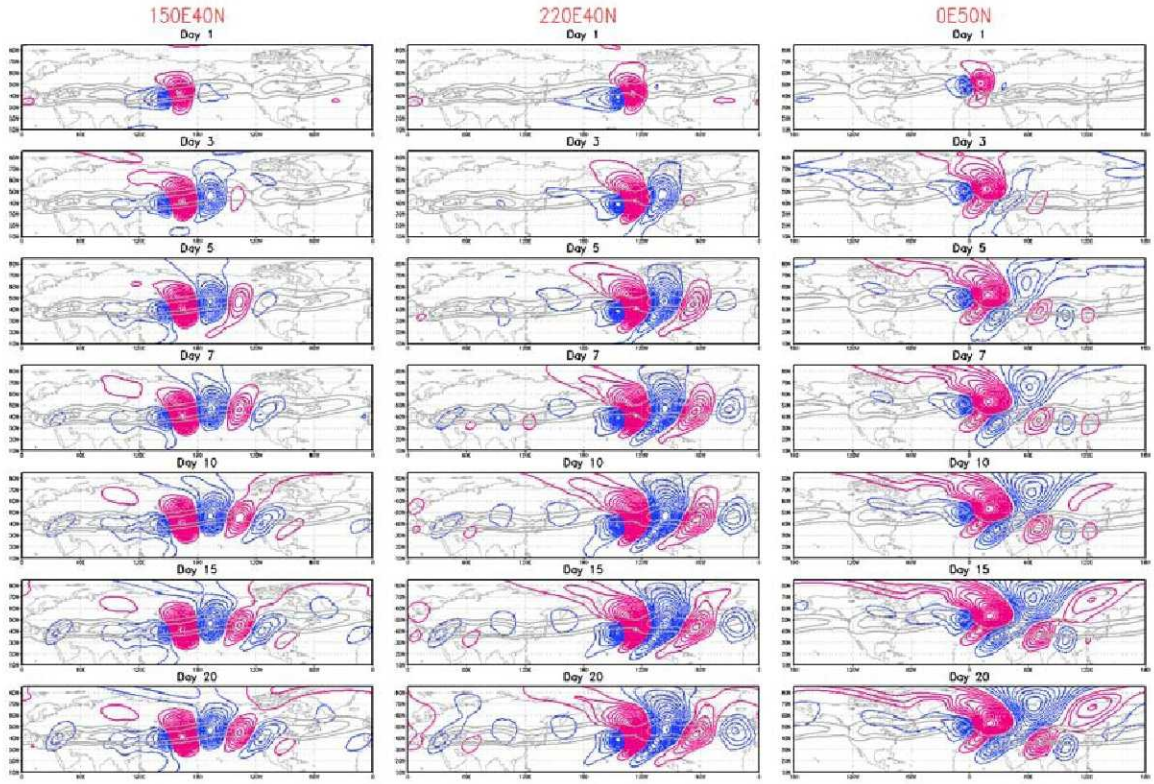

Figure 11: The time evolution of the response of the eddy v-wind at σ=0.257 to an idealized vorticity source at 150E, 40N (left panels), 220E, 40N (middle panels), and 0E, 50N (right panels). The results are from a stationary wave model with a 3-dimensional JJA mean base state taken from MERRA for the period 1979-2010. See text for details of the forcing. Contour interval is 0.08 m/s.

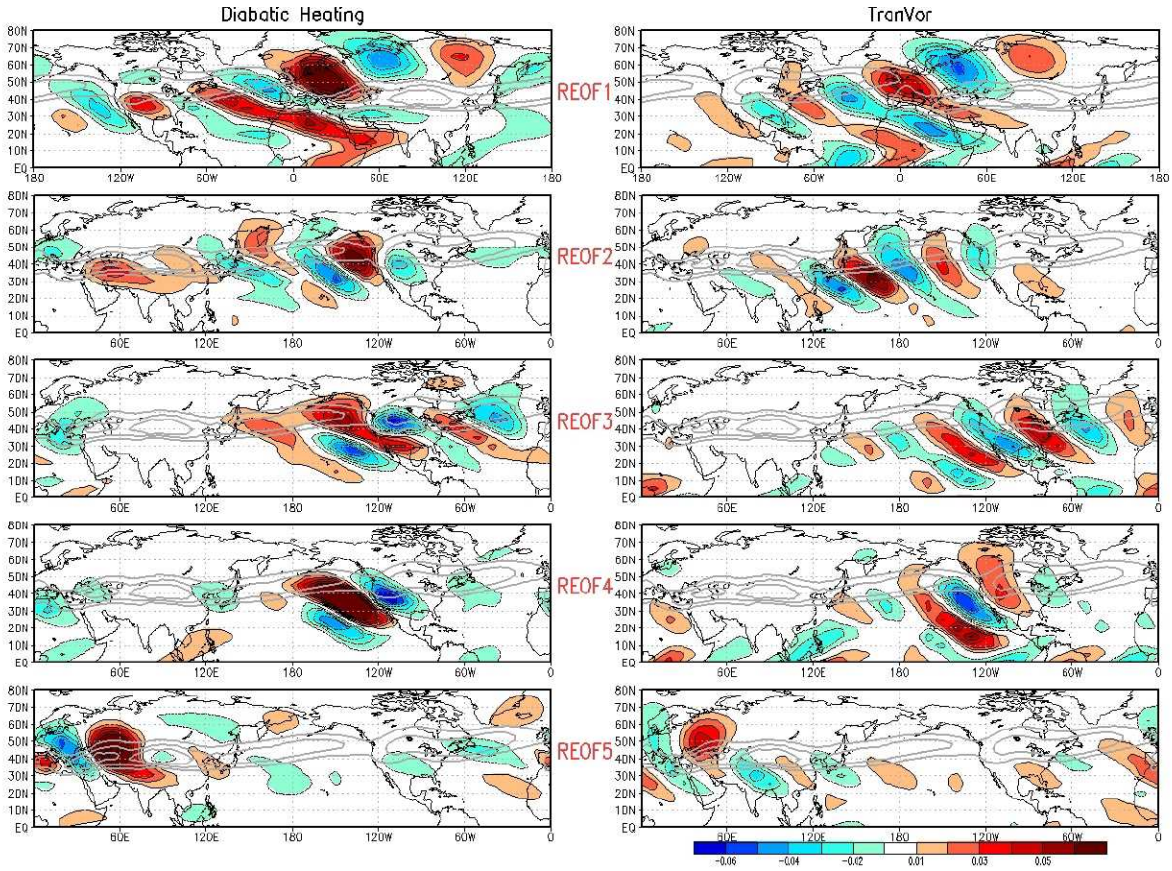

Figure 12: The optimal forcing regions for the 5 leading REOFs based on the stationary wave model results using a JJA 1979-2010 mean three-dimensional base state from MERRA. The left panels show the optimal patterns for the heating, while the right panels show the optimal patterns for vorticity. The patterns are computed as the inner product between the eddy v-wind response at σ=0.257 to the forcing and the REOFs (see text for details). Units are arbitrary.

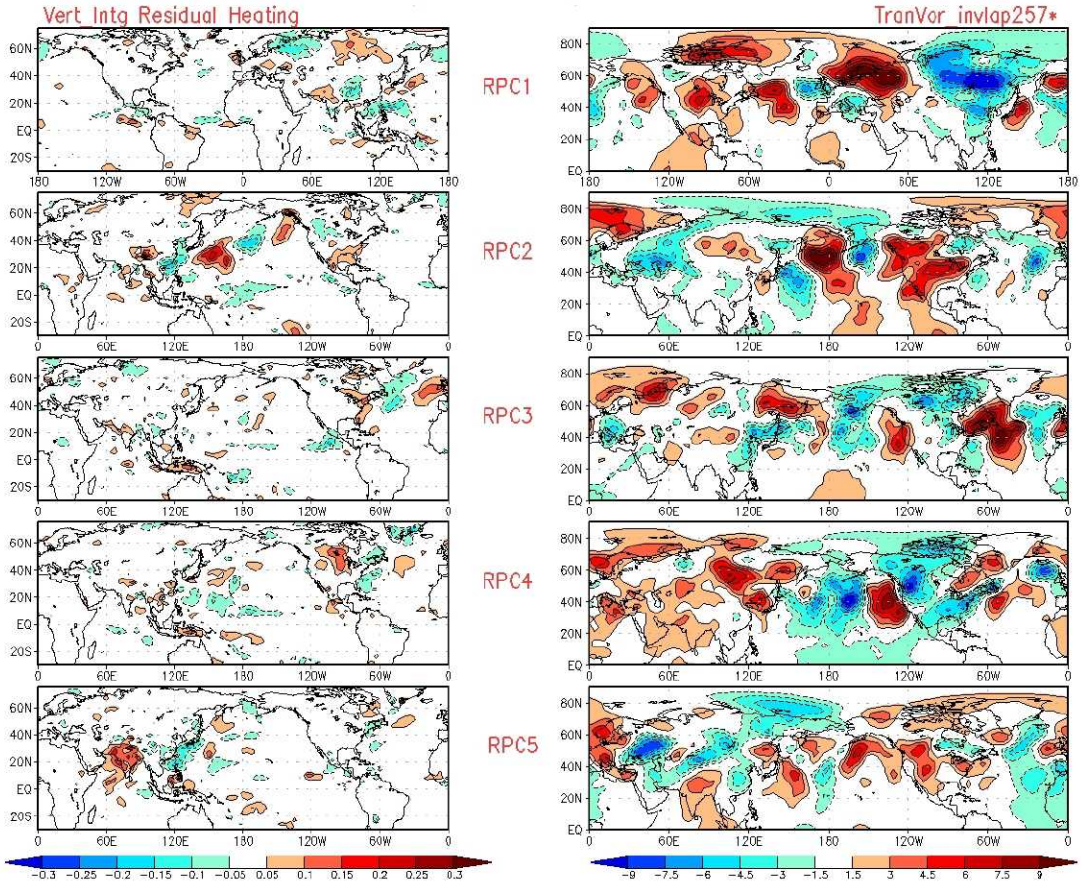

Fig. 13: Vertically integrated heating (left panels) and eddy (zonal mean removed) transient vorticity forcing at σ=0.257 (right panels) estimated from MERRA associated with each REOF. The results are based on a simple linear regression at each grid point in which the predictor is the REOF and the predictand is the subseasonal forcing. The results are plotted assuming one standard deviation in the RPCs. Units in the left panels are °K/day. The transient vorticity forcing fields are smoothed by applying the inverse Laplacian (units are m^2 s^{-2}).

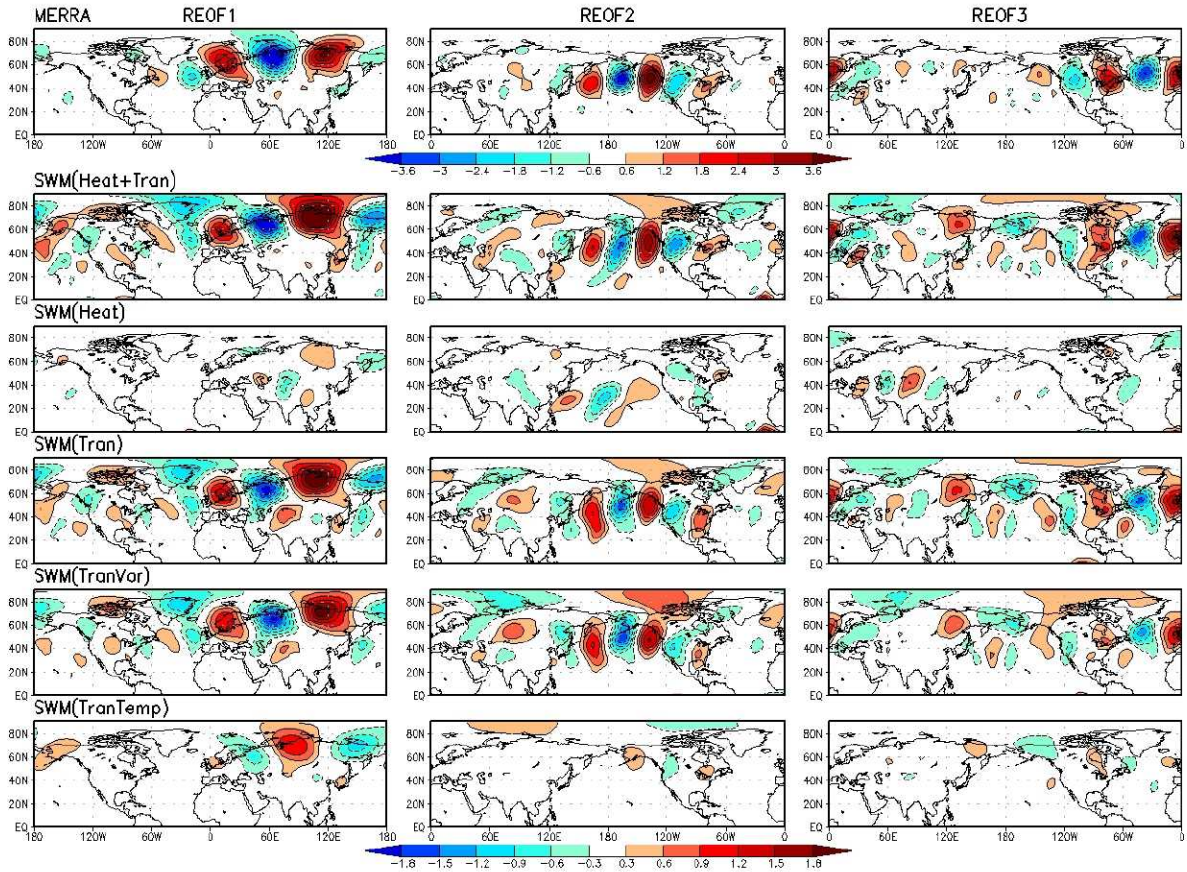

Fig. 14a: The first row is the subseasonal monthly JJA V250mb v-wind regressed against the three leading REOFs, and plotted assuming one standard deviation in the REOFs. The remaining rows are the responses to the estimated forcing terms for the first (left panels), second (middle panels) and third (right panels) REOFs. The second from the top row is the response to the total forcing. The third row is the response to the heating. The fourth row shows the response to the total (temperature plus vorticity plus divergence) transient forcing. The fifth and sixth rows show the separate responses to the vorticity and temperature transients, respectively. Units: m/s.

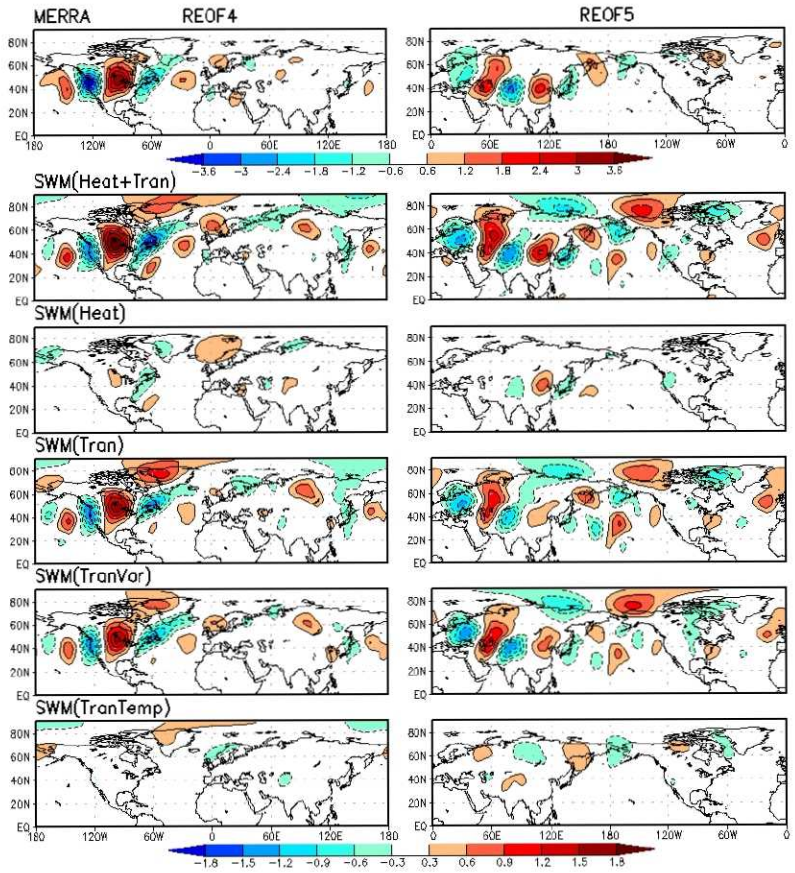

Fig. 14b: Same as Fig. 14a, except for the fourth (left panels) and fifth (right panels) leading REOFs.